Weighted Joint Bilateral Filter with Slope Depth Compensation Filter for Depth Map Refinement

Takuya Matsuo[1], Norishige Fukushima[1] and Yutaka Ishibashi[1]
[1]*Graduate School of Engineering,*
Nagoya Institute of Technology,
Gokiso-cho, Showa-ku, Nagoya 466-8555, Japan
t-matsuo@mcl.nitech.ac.jp, {fukushima, ishibasi}@nitech.ac.jp

Keywords: depth map refinement, stereo matching, depth sensor, weighted joint bilateral filter, real-time image processing

Abstract: In this paper, we propose a new refinement filter for depth maps. The filter convolutes a depth map by a jointly computed kernel on a natural image with a weight map. We call the filter weighted joint bilateral filter. The filter fits an outline of an object in the depth map to the outline of the object in the natural image, and it reduces noises. An additional filter of slope depth compensation filter removes blur across object boundary. The filter set's computational cost is low and is independent of depth ranges. Thus we can refine depth maps to generate accurate depth map with lower cost. In addition, we can apply the filters for various types of depth map, such as computed by simple block matching, Markov random field based optimization, and Depth sensors. Experimental results show that the proposed filter has the best performance of improvement of depth map accuracy, and the proposed filter can perform real-time refinement.

1 INTRODUCTION

Recently, image processing with depth maps (e.g. pose estimation, object detection, point cloud processing and free viewpoint video rendering) attracts attentions, and releases of consumer-level depth sensors (e.g. Microsoft Kinect and ASUS Xtion) accelerate the boom. In these applications, accurate depth maps are required. Especially, the free viewpoint image rendering requires more accurate depth maps (Fukushima and Ishibashi, 2011). The free viewpoint images are often synthesized by depth image based rendering (DIBR) (Mori et al., 2009) that demands input images and depth maps.

Depth maps are usually computed by stereo matching with stereo image pair. The stereo matching finds corresponding pixels between left and right images. The depth values are computed from disparities of the correspondence. The stereo matching consists of four steps that are matching cost computation, cost aggregation, depth map computation/optimization and depth map refinement (Scharstein and Szeliski, 2002).

Depth maps computed by stereo matching methods tend to have invalid depth value around object edges and contain spike/speckle noise. To obtain accurate depth maps, most of the stereo matching methods perform an optimization to improve the accuracy of the depth map.

The optimization methods based on Markov random field/conditional random field (e.g. dynamic programming (Ohta and Kanade, 1985), multi-pass dynamic programming (Fukushima et al., 2010), semi-global block matching (Hirschmuller, 2008), belief propagation (Sun et al., 2003) and graph cuts (Boykov et al., 2001)), generate accurate depth maps, while these complex optimizations consume much time. The computational cost depends on search range of depths or disparities. The computational order is usually $O(d)$, $O(d \log d)$ or $O(d^2)$, where d is search range of disparities/depths. In addition, the strong constrains of the smoothness consistency in the optimizations tend to obscure local edges of the depth map. (Wildeboer et al., 2010) solves the problem by using manual user inputs which indicate object edges.

To make real-time stereo matching, we can select light weight algorithms, but its accuracy does not reach well optimized approaches, so depth map at object boundaries will be invalid and large noises will appear. Thus, computational cost and accuracy are trade-off problem,

Depth sensors, including IR signal pattern projection based and Time of Flight (ToF) based sensors, also generate depth maps. These devices can cap-

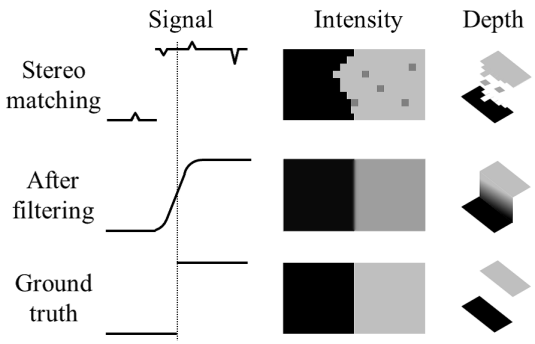

Figure 1: Effect of depth map refinement.

ture more accurate depth maps, but they cannot capture natural RGB images. To capture RGB images, an additional CCD sensor is required. In addition depth map-image registration is required because sensors' positions are different. However, the registration tends to be violated at object boundaries.

In the real-time stereo matching and the depth sensor acquisition, both methods require noise reduction, object boundaries recovering are required. Therefore, to correct the depth at object boundary, and to remove noise on depth maps, we propose a refinement filter for depth maps from stereo image pair or depth sensors. For real-time applications, we keep the computational cost of the filter low.

The rest of this paper is organized as follows. Sec. 2 describes related works of refinement filters. Proposed methods are presented in Sec. 3, and experimental results are shown in Sec. 4. Sec. 5 concludes this paper.

2 RELATED WORKS

Recently, depth map refinement filters are focused. Requirements for the refinement filter are; capability of edge correction, noise reduction, and edge keeping. Figure 1 shows the effect of depth map refinement. Input depth signals are noisy and edge at boundary is not correct. After refinement filter, noise on depth signal is removed and depth at boundary is corrected. However unwanted slope blur at the boundary occurs. The slope means that object boundary is smoothly connected, but this is a fake signal. Thus keeping the blur size small or removing the blur is important for the refinement.

The depth map refinement filters are often edge-preserving filter, e.g. median filter. Bilateral filter (Tomasi and Manduchi, 1998) is an early approach of them. The bilateral filter can remove noise while preserving edges, but the performance of edge keeping and noise reduction is trade-off. When the image has large noises, the performance of edge keeping becomes low to remove the noises. In addition, only Gaussian noise can be removed by the filter, although depth map contains spike, speckle/blob and non-Gaussian noises. Moreover, the inaccuracy around object boundaries cannot be correct well.

Now, a variant called joint bilateral filter (or cross bilateral filter) (Pestschnigg et al., 2004; Eisemann and Durand, 2004; Kopf et al., 2007) relaxes bilateral filter's problem well by adding additional information. The information is an original RGB image used in depth estimation. This method regards the depth map as a filtering target, and the original RGB image as a kernel computation target. The filter makes the kernel by color or intensity values of the RGB image instead of depth values. The filter can smooth small non-Gaussian noises. In addition the filter can fit edges in the depth map around an object to edges in the natural image's object. However, the joint depth and image processing make a new problem. The joint bilateral filter spreads blurring to the outside of the depth map due to mixed pixels, and outliers. Mixed pixels in natural images occur on foreground and background boundaries and they are caused by CCD sensor's aliasing and optical lens blur. The joint bilateral filter transfers the blur to the depth map. In addition, impulse outliers and large size noises on the depth map are diffused by the filtering.

Some methods can reduce this type of the blur in some degree. Multilateral filter (Lai et al., 2010) has three weights which are space, color and additional depth weight. The depth weight wants to keep the shape of the edge of the depth map so that the weight suspends blurring. Unfortunately, the weight also loses an ability of the object boundary recovering.

Cost volume based refinement filter (Yang et al., 2007) and its speedup approximation (Yang et al., 2010) have better performance. The methods can correct depth edge and can remove spike noise and small size speckle noise without diffusion. In addition the method hardly generates blur at object boundaries. In the processing of the cost volume filter, cost slices which indicate every possibility of a depth value at each pixel is computed, and all slices of each depth level are stacked. The set of stacked slices are called cost volume. Then, each slice is filtered by the joint bilateral filter slice by slice at each depth level. The possibility is computed by a difference between an initial depth and each depth level values. The method performs d (depth search range) times bilateral filters, and also iterates the multiple bilateral filtering process. Thus the method consumes a lot of time.

The refinement filter which meets all requirements is only cost volume refinement, but it is cost consuming. Thus a fast filter which meets all requirements is an open question. Therefore, we present a new refinement filter to remove impulse/speckle noises, recover object shapes and suppress the blurs with low computational cost. The refinement contains two filters; one is weighted joint bilateral filter which is a variant of joint bilateral filter and can reduce the boundary's blurs size, and the other is the slope depth compensation filter which eliminates depth slopes or blurs between a foreground and background objects.

3 PROPOSED FILTER

3.1 Weighted joint bilateral filter

Our filter can reduce noises and correct object boundaries without large blur by using an input natural image and a depth map. The filter is a variant of the joint bilateral filter, and we call the filter *weighted joint bilateral filter (WJBF)*.

We add a weight factor to the joint bilateral filter. The filter is defined by the following formula:

$$D_{\boldsymbol{p}} = \frac{\sum_{\boldsymbol{s}\in N} w(\boldsymbol{p},\boldsymbol{s})c(I_{\boldsymbol{p}},I_{\boldsymbol{s}})R_{\boldsymbol{s}}D_{\boldsymbol{s}}}{\sum_{\boldsymbol{s}\in N} w(\boldsymbol{p},\boldsymbol{s})c(I_{\boldsymbol{p}},I_{\boldsymbol{s}})R_{\boldsymbol{s}}}, \quad (1)$$

$$w(\boldsymbol{x},\boldsymbol{y}) = e^{-\frac{1}{2}(\frac{||\boldsymbol{x}-\boldsymbol{y}||_2}{\sigma_s})}, c(\boldsymbol{x},\boldsymbol{y}) = e^{-\frac{1}{2}(\frac{||\boldsymbol{x}-\boldsymbol{y}||_2}{\sigma_c})},$$

where $\boldsymbol{p}$ = coordinate of current pixel, $\boldsymbol{s}$ = coordinate of support pixel centered around pixel $\boldsymbol{p}$, I = input natural image, D = input/output depth map, N = aggregating set of support pixel $\boldsymbol{s}$, w = spatial kernel weight function, c = color/range kernel weight function, and each weight function is Gaussian distribution (σ_s, σ_c: const.). $||\cdot||_2$ is L2 norm function, and $R_{\boldsymbol{s}}$ = weight map. This filter is an equivalent joint bilateral filter except for the weight map R. If the weight map is uniform, for example all values of the weighted map are set to 1, the weighted joint bilateral filter becomes the joint bilateral filter.

The Eq. (1) is separated into 2 parts; one is a kernel weighting part and the other is a weighting of values of filtering target part. The former is w and c, and the latter is R. The value's weight R controls amount of influence of depth value on a pixel and is fixed over the image filtering. Thus we should set high weight at a pixel which has a reliable depth value.

We want to set the joint bilateral kernel weight of support pixels on another object to no weight. In the joint bilateral filter case, the kernel weight between a current pixel locates on an object boundary and support pixel on another object tend to have medium kernel weight due to a mixed pixel on the object boundary.

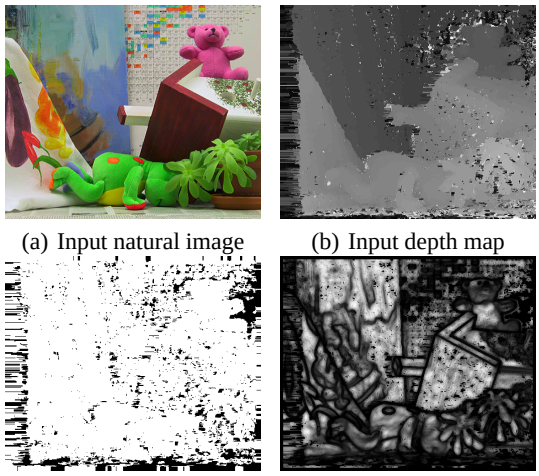

(a) Input natural image (b) Input depth map

(c) Speckle mask (d) Weight map

Figure 2: Example of weight map.

The unwanted weight causes blurs on the depth map near the object boundary. The depth values around the object discontinuities are unreliable, so we should set the weight of the depth value R to low.

In addition, impulse outliers or outliers in speckles/blobs are unreliable. Small speckles may be miss estimated regions. The region should be set to no weight. Figure 2(b) shows an example of impulse or speckles/blobs in a depth map. If we cannot ignore these regions, the regions of speckle noise are diffused by a smoothing filter. Basically, the object boundary and the speckle region adversely affect depth map refinement. Thus we make a weight value for every pixel, which is a weight map R, in advance to softly ignore the ambiguous regions of the object boundary and the speckle region.

In the weight map computation process, we classify pixels into located around object boundaries or not, and speckle noise or not pixels. The result of the soft classification is represented by weighting values. In the classification process, we have two assumptions: First, if there is no boundary between the current pixel and the support pixel, both pixels are located at the same object. In this case, the depth value and the intensity/color of the current pixel are similar to these of the support pixels. Second, if size of a connected component is small, the region is speckle noised. In the connected component, difference among depth values is low.

Under the assumptions, the weight value R at $\boldsymbol{s}$ is:

$$R_{\boldsymbol{s}} = \sum_{\boldsymbol{s}\in N'} M_{\boldsymbol{s}} \cdot w(\boldsymbol{s},\boldsymbol{q})c(I_{\boldsymbol{s}},I_{\boldsymbol{q}})e^{-\frac{1}{2}(\frac{||D_{\boldsymbol{s}}-D_{\boldsymbol{q}}||_2}{\sigma_r})}, \quad (2)$$

where $\boldsymbol{q}$ = coordinate of support pixel centered around pixel $\boldsymbol{s}$, N' = aggregating set of support pixel $\boldsymbol{q}$, $w(\boldsymbol{s},\boldsymbol{q})$ and $c(I_{\boldsymbol{s}},I_{\boldsymbol{q}})$ are same functions as (1). How-

ever, equation (2) has an additional term of the difference of the depth values between the current and the support pixel. M_s is a speckle region mask. The speckle mask has two weight values which is 0 and 1. The areas of weight value 0 are the speckle regions, and the areas of weight value 1 are non-speckle regions.

The first assumption is calculated by distance of the intensity and the depth value of between the current pixel and the support pixels. The second assumption of the speckle regions is represented by the speckle mask. This mask is made by the initial depth map using the speckle detection filter. The speckle detection filter has two parameters. They are upper threshold of speckle component size (*speckleWindowSize*) and allowable difference range in the speckle (*speckleRange*). The speckle detection filter judges region to be a speckle by whether or not the region size is smaller than the speckle window size and the region value is larger than the speckle range. If some areas judged the speckle regions by the speckle detection filter in the initial depth map, the weight of the speckle region is set to 0.

Figure 2 shows examples of an input image, a noisy depth map, a speckle mask and a weight map. If regions are speckled pixels, the speckle regions have no weight. If not, all value of M_s is set to 1, so the weight map has some weight values. As a result, boundary regions in the images and the depth map have small weight. We can softly ignore boundary's depth values and speckle's depth values, therefore, the weighted bilateral filter with the weight map can suppress boundary blur, can correct image boundary well, and can reduce the speckle noises.

In the brute force computation of the filtering a pixel has the fourfold loops (vertical and horizontal filtering kernel and vertical and horizontal weight map kernel loops), but the weight map is constant in Eq. (1). Thus we compute the weight map before the weighted joint bilateral filtering for effective computation.

3.2 Slope depth compensation filter

The weighted joint bilateral filter refines accuracy around boundaries and smoothness on flat regions, but subtle blurs still remain in such cases, e.g. difference between foreground and background color is small, and/or difference between foreground and background depth value is large. The depth values around the boundary are usually almost binary (foreground/background); thus averaged depth values are not suitable. The blurs make slopes between the foreground and background depths. They do not exist in the real environment. Consequently, these slopes

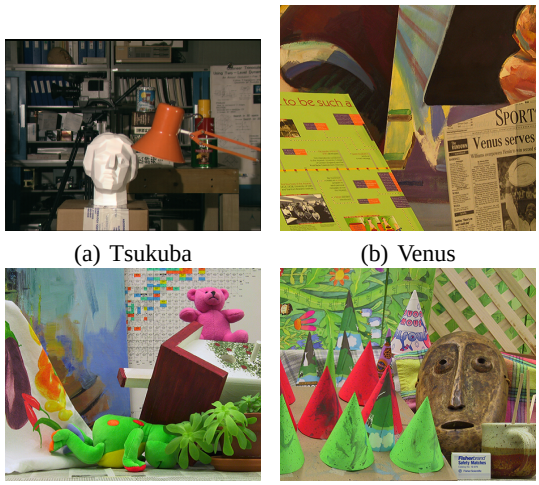

(a) Tsukuba (b) Venus

(c) Teddy (d) Cones

Figure 3: Middlebury's data sets.

should be removed. We propose a new filter called *Slope depth compensation filter (SDCF)*.

The filter is defined by the following formula:

$$\begin{aligned} D_{\boldsymbol{p}}^{SDCF} &= D_{\boldsymbol{v}}^{INITIAL} \\ \text{s.t.} \quad \boldsymbol{v} &= \arg\min_{s \in W} ||D_{\boldsymbol{p}}^{WJBF} - D_{\boldsymbol{s}}^{INITIAL}||_2, \end{aligned} \tag{3}$$

where D^X is the depth map estimated by a method $X \in \{INITIAL, WJBF, SDCF\}$, W is the aggregation set of a support pixel, $|\cdot|_2$ means L2 norm function, $\boldsymbol{p}$ is target pixel position, $\boldsymbol{s}$ is support pixel position, and $\boldsymbol{v}$ is a pixel position which points the minimum of the function.

This filter replaces the values blurred by the weighted joint bilateral filter as the nearest values in the support region on the no filtered version of $D^{INITIAL}$. There are not mixed values in no filtered version so that the filter completely removes blended values.

At first, the depth map $D^{INITIAL}$ is obtained by a stereo matching method, and then the depth map is filtered by the weighted joint bilateral filter (output is written as D^{WJBF}), and finally the depth map is compensated by depth slope compensation filter (D^{DSCF}).

4 EXPERIMENTAL RESULTS

4.1 Experimental setups

We evaluate the weighted joint bilateral filter (WJBF) with the slope depth compensation filter (SDCF). The combination of WJBF and the SDCF is called proposed method (in short Proposed). In our experiments, we evaluate accuracy improvement of the pro-

Table 1: Error Rate (%) of depth maps: Results of various stereo matching methods (block matching (BM), dynamic programming (DP), semi-global block matching (SGBM), efficient large scale stereo (ELAS), and double belief propagation (DBP)) with proposed filter or refinement filters (median filter (MF), bilateral filter (BF), joint bilateral filter (JBF), multi lateral filter (MLF), and filter in constant space belief propagation (CSBP)).

	Tsukuba			Venus			Teddy			Cones		
	nonocc	all	disc	nonocc	all	disc	nonocc	all	disc	nonocc	all	disc
BM_h	10.78	12.22	20.03	12.58	13.79	23.06	16.17	24.25	29.89	7.76	17.19	20.01
BM_h & WJBF	3.39	4.21	13.95	1.69	2.60	13.66	12.18	20.63	24.04	3.94	12.38	11.78
BM_h & Proposed	3.25	4.04	13.15	1.36	2.07	9.51	9.20	17.55	20.20	3.03	11.38	9.04
BM_m	7.50	8.75	18.84	5.01	5.96	16.49	12.36	18.10	24.94	5.56	11.54	15.47
BM_m & WJBF	3.14	3.78	14.59	2.62	3.17	8.52	10.09	15.84	21.84	4.57	10.43	13.67
BM_m & Proposed	2.89	3.45	13.29	1.49	1.94	4.22	8.79	14.24	19.22	3.13	8.53	9.21
BM_l	4.60	5.93	17.99	2.08	2.91	16.11	10.63	15.51	26.43	4.97	10.46	14.31
BM_l & WJBF	2.69	3.20	12.57	1.51	2.14	9.55	9.41	14.41	22.56	4.61	10.08	13.52
BM_l & Proposed	2.54	3.25	11.53	1.03	1.50	5.11	8.90	13.71	21.05	3.25	8.43	9.62
DP	4.12	5.04	11.95	10.10	11.03	21.03	14.00	21.58	20.56	10.54	19.10	21.10
DP & WJBF	2.63	3.40	11.12	6.77	7.17	20.65	9.81	17.12	18.44	7.98	15.92	18.49
DP & Proposed	2.49	3.22	10.74	6.01	6.36	18.12	9.22	16.53	16.98	7.12	15.64	16.05
SGBM	3.98	5.56	15.47	1.33	2.59	15.23	7.60	14.83	20.90	4.55	11.33	12.81
SGBM & WJBF	2.42	3.09	9.83	0.46	0.97	5.02	6.33	13.41	17.53	3.89	10.22	11.58
SGBM & Proposed	2.34	2.59	9.42	0.36	0.83	3.73	5.68	12.43	15.42	2.58	8.62	7.68
ELAS	3.99	5.45	18.14	1.84	2.55	20.28	7.99	14.69	22.33	6.85	14.55	17.30
ELAS & WJBF	2.96	3.68	13.33	0.71	1.18	7.82	6.55	13.23	17.60	5.35	12.80	13.90
ELAS & Proposed	2.87	3.54	12.86	0.55	0.81	5.65	6.07	12.48	15.67	4.58	12.04	11.69
DBP	0.88	1.29	4.76	0.13	0.45	1.87	3.53	8.30	9.63	2.90	8.78	7.79
DBP & WJBF	0.88	1.31	4.78	0.15	0.39	2.04	3.57	8.37	9.80	2.97	8.74	8.05
DBP & Proposed	0.83	1.19	4.78	0.10	0.32	1.44	3.56	8.31	9.69	2.87	8.62	7.74
BM_l & MF	3.54	4.72	16.96	1.50	2.32	16.12	10.35	15.41	25.96	4.52	9.99	13.16
BM_l & BF	3.92	5.29	16.73	1.77	2.63	16.90	10.51	15.42	26.21	4.76	10.24	13.91
BM_l & JBF	4.57	5.82	19.37	2.14	2.98	16.64	11.50	17.17	29.37	6.77	12.37	19.59
BM_l & MLF	4.25	5.34	18.02	2.73	3.74	26.08	11.45	17.15	29.17	6.54	12.04	18.93
BM_l & CSBP	4.79	6.56	17.68	2.42	3.40	21.17	11.31	16.08	28.81	5.49	11.31	15.55

posed filter for various types of depth map. In addition, we reveal advantage of its computational cost. Moreover we show an example of refinement of depth map from Microsoft Kinect.

We use the Middlebury's data sets (Scharstein and Szeliski, 2002) are used for our stereo evaluation in the experiments. Data sets are Tsukuba, Venus, Teddy and Cones (Fig. 3). The image resolution and depth search range of each image are Tsukuba ($384 \times 288, 16$), Venus ($434 \times 383, 32$), Teddy and Cones ($450 \times 375, 64$), respectively.

We evaluate the proposed refinement filter for various depth inputs. Stereo matching methods for the input depth maps are block matching (BM), dynamic programming (DP) (Ohta and Kanade, 1985), semi-global block matching (SGBM) (Hirschmuller, 2008), efficient large-scale stereo (ELAS) (Geiger et al., 2010) and double belief propagation (DBP) (Yang et al., 2008).

We prepared three patterns of the BM's depth map according to the amount of noises. They are high (BM_h), middle (BM_m) and low noise depth maps (BM_l) (See Figs. 6(a), 6(d), 6(g)). The characteristics of the other depth maps are as follows. The DP, SGBM and ELAS are computed by stereo method which has near real-time performance, whose depth maps are middle accuracy (See Figs. 7(a), 8(a), 9(a)). The DBP (10(a))) is the most accurate method but it takes much time (several minutes).

Table 2: Comparing proposed method with cost volume refinement (Teddy).

	nonocc	all	disc
BM_h	16.17	24.25	29.89
BM_h & CVR	8.15	16.25	20.49
BM_h & Proposed	9.20	17.55	20.20
BM_l	10.63	15.51	26.43
BM_l & CVR	8.98	13.58	21.58
BM_l & Proposed	8.90	13.71	21.05
SGBM	7.60	14.83	20.90
SGBM & CVR	5.93	12.93	16.39
SGBM & Proposed	5.68	12.43	15.42

In addition, the effect of the proposed refinement filter is verified by following competitive refinement filters. These are the low noise BM's depth map with median filter (MF), bilateral filter (BF) (Tomasi and Manduchi, 1998), joint bilateral filter (JBF) (Pestschnigg et al., 2004; Eisemann and Durand, 2004; Kopf et al., 2007), multilateral filter (MLF) (Lai et al., 2010) and speedup version of (Yang

et al., 2007) used in constant space belief propagation (CSBP) (Yang et al., 2010) are used as refinement filters. Furthermore, we compare our proposed method with a cost volume refinement method (Yang et al., 2007). In the cost volume refinement, we use joint bilateral filter for cost slice filtering, and we use inputs depth maps with BM_h, BM_l and SGBM.

4.2 Results

The resulting depth maps are shown in Fig. 6 to Fig. 11 (only Teddy's results are shown due to the room of the space at the end of the paper). There are five parameters at weighted image generation and two parameters at filtering. The parameters of proposed method at weighted image generation are $(\sigma_s, \sigma_c, \sigma_r, speckleWindowSize, speckleRange) = (15.4, 5.1, 1.4, 38, 1)$, and those at filtering are $(\sigma_s, \sigma_c) = (15.3, 10.7)$ using BM_h depth map. There parameters are experimentally determined in all cases. The results of error rate are shown in Tab. 1. We use the error rate defined in (Scharstein and Szeliski, 2002). It is calculated by a percentage of the error pixel of input depth map. Difference between the input depth map and the ground truth depth map in the error pixel has over a threshold value (set to 1 in these experiments). In Tab. 1 and Tab. 2, "nonocc", "all" and "disc" locate different region, respectively. The header row "nonocc" evaluates in non-occluded regions. The header row "all" evaluates in all regions. The header row "disc" evaluates in regions near depth discontinuities.

In Table 1, our proposed method can improve accuracy in all competitive stereo matching methods and in any data sets, except for DBP. Especially, amount of the improvement is bigger when accuracy of depth maps is low. Such roughly estimated depth maps contain a lot of region of estimation error and obscure edges. Thus, the proposed method works well for these depth maps because of noise reduction and correcting object boundary ability. But, as for an accurate depth map, such as DBP, the proposed method has almost no effect. This is because that there is no region which is possible to be improved. Instead, in some cases, the error rate is increasing according to generated invalid depth value by mixing some depth values.

Moreover, Table 1 shows that the effect of using only WJBF and using the proposed method (WJBF + SDCF). The effect of the WJBF becomes higher when the accuracy of input depth map is low. This is because that the WJBF removes the whole noise, but the SDCF compensate only blurred edge. Thus, these methods differ in the effect range greatly.

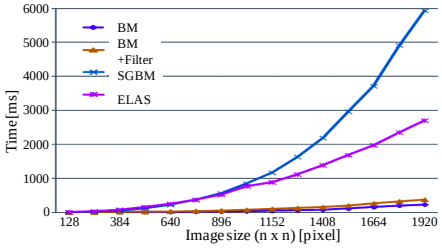

(a) Y axis is until 6000 ms

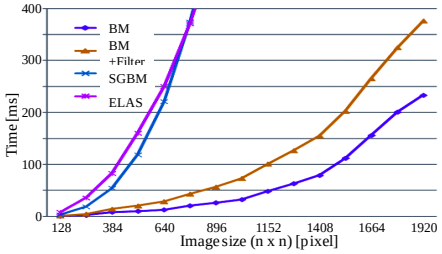

(b) Y axis is until 400ms

Figure 4: Computational time of each method.

In addition, our proposed refinement filter has the best performance among all competitive refinement filters (cost volume refinement is discussed later). This is because that the MF and the BF can reduce noise, but, cannot correct object edges. The JBF and the MLF can reduce noise and correct object edges, but cannot correct all blur on edges according to mixing some depth values. On the other hands, proposed method can reduce noise, correct object edges and control edge blurring.

Here, the effect of the proposed method is considered from Fig. 6 to Fig. 10. In Fig. 6, depth maps of (a), (d) and (g) is input depth map with BM. Each depth map is low accuracy which has many noise and incorrect object edges. Depth maps of (b), (e) and (h) are refined by WJBF. These depth maps are reduced noise and corrected object edges through the WJBF. But, blur edges occur in object boundary. Whereat using SDCF, the blur of boundary edges is compensated in depth maps of (c), (f) and (i). The same effect is shown by Fig. 7 to Fig. 9. In Fig. 7(a), the effect of noise reduction is shown. A noise of estimation error using the DP is reduced by the WJBF. Also, the effect of edge correction is shown in Fig. 8 and Fig. 9. An irregularity of boundary edges is corrected by SDCF. On the other hands, the effect of our proposed method is not shown in Fig. 10(a). A depth map of (a) using DBP has almost no noise and correct edges. Thus, our proposed method hardly makes an effect.

Here, we consider our proposed method and the cost volume refinement method (CVR). Table 2 and Fig. 12 show performance of CVR. The input depth maps are BM_h, BM_l and SGBM and we use Teddy

Table 3: Comparing running time (ms) of BM plus proposed filter with selected stereo methods. Kernel size is 7×7.

Data Set	BM	Proposed	BM+Proposed	SGBM	ELAS
tsukuba	5.7	4.1	9.8	28.8	61.1
venus	8.4	6.1	14.5	45.9	110.0
teddy and cones	10.5	7.4	17.9	71.4	168.2

data set (Other data sets have the almost same tendency). Comparing the CVR with the proposed method with each depth map inputs, the performance of the proposed method is the same or better than CVR with BMl and SGBM. In the highest noise case, CVR has the better performance than the proposed filter. Thus CVR has strong noise reduction performance but reduce some detail.

The notable factor of CVR is computational cost. The cost volume is calculated by stacking the cost slice of the each depth value which is difference between an input depth and each depth values, and, filters every stack. Thus, this method is expensive. For example, 64 times bilateral filtering is required in Teddy case, and about 32 times slower than the proposed method. Our proposed method has real-time capability. Therefore, if the accuracy of an acquired depth maps is comparable, our proposed method is more effective than CVR.

Table 3 and Fig. 4 show the result of the running time with Intel Core i7-920 2.93GHz. Here, competitive methods are SGBM and ELAS which are near real-time methods in optimized methods. The BM with the proposed method is faster than the SGBM and the ELAS for any data set. In addition, refinement filters depend only on the image resolution, while optimization processes (e.g. SGBM) depend also on the depth search range; thus the gap of the running time between the proposed method and optimized method like the SGBM more increase as the image resolution and the search range become larger. Recently, image and display resolution are rapidly improved, thus the proposed method is favorable. Figure 4 shows computational time of various size of simulate image data. The lowest size of the input image is 128×128 and its search range is 8. The input images are generated by multiplying the minimum size image, such as $(256 \times 256, 16)$, $(384 \times 384, 24)$, ..., $(1920 \times 1920, 120)$. The results show that BM is quite faster than the SGBM and ELAS, and the computational cost of the proposed refinement filter is quite low.

We can also use the proposed filter for depth maps from Microsoft Kinect. Figure 5 shows experimental results of a depth map from Kinect depth sensor, and the sequence is uploaded by (Lai et al., 2011). In this experiment, we refine the depth map from the Kinect depth sensor and synthesis a free viewpoint image.

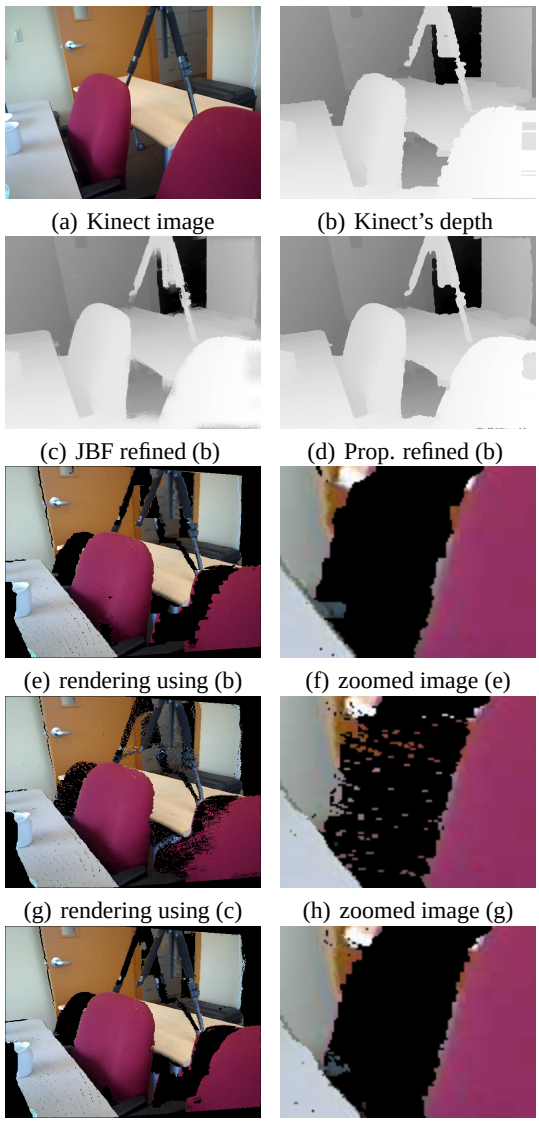

(a) Kinect image (b) Kinect's depth
(c) JBF refined (b) (d) Prop. refined (b)
(e) rendering using (b) (f) zoomed image (e)
(g) rendering using (c) (h) zoomed image (g)
(i) rendering using (d) (j) zoomed image (i)

Figure 5: Results of refined depth map and warped view from Kinect depth map.

The free viewpoint image synthesis is performed by the depth image based rendering (Mori et al., 2009). The non-filtered depth map of getting the Kinect has rough edges (Fig. 5(b)). Thus, the edge of a composite image which uses non filtered depth map is defectiveness (See the chair region of Fig. 5(e, f)). The depth filtered by joint bilateral filter has blurs around the boundary (Fig. 5(c)), the render-

ing images are scattered around the object boundary (Fig. 5(g, h)). In contrast, the depth map filtered by the proposed filter has corrected edges and no blurs (Fig. 5(d)). As a result, the edge of the composite image (Fig. 5(i), (j)) is more corrective then the non-filtered or joint bilateral filtered it.

5 CONCLUSIONS

In this paper, we proposed a refinement filter set for depth map improvement—called weight joint bilateral filter and slope depth compensation filter. The proposed method can reduce depth noise and correct object boundary edge without boundary blurring, and it has real-time performance. Experimental results showed that our proposed filter can improve accuracy of depth maps from various stereo matching methods, and has the best performance among the comparative refinement filters. Especially, amount of improvement is large when an input depth map is not accurate. In such case, computational time of a stereo matching method is low. Exception case is using fairly optimized depth map, such as double belief propagation. However the method takes a lot of time. In addition, its computational speed is faster than the fastest Markov random field optimization algorithm of semi-global block matching. Moreover, the filter can apply the depth map from Kinect, and then the quality of the synthesized image is up.

In our future work, we will investigate dependencies of input natural images and depth maps, and verify the proposed filter's parameters.

ACKNOWLEDGMENT

The authors thank Prof. Shinji Sugawara for valuable discussions. This work was partly supported by the Grand-In-Aid for Young Scientists (B) of Japan Society for the Promotion of Science under Grant 22700174, and SCOPE (Strategic Information and Communications R&D Promotion Programme) 122106001 of the Ministry of Internal Affairs and Communications of Japan.

REFERENCES

Boykov, Y., Veksler, O., and Zabih, R. (2001). Fast approximate energy minimization via graph cuts. *IEEE Trans. PAMI*, 23(11):1222–1239.

Eisemann, E. and Durand, F. (2004). Flash photography enhancement via intrinsic relighting. *ACM Trans. on Graphics*, 23(3):673–678.

Fukushima, N., Fujii, T., Ishibashi, Y., Yendo, T., and Tanimoto, M. (2010). Real-time free viewpoint image rendering by using fast multi-pass dynamic programming. In *3DTV-Conference: The True Vision-Capture, Transmission and Display of 3D Video (3DTV-CON)*, pages 1–4.

Fukushima, N. and Ishibashi, Y. (2011). Client driven system of depth image based rendering. *ECTI Trans. CIT*, 5(2):15–23.

Geiger, A., Roser, M., and Urtasun, R. (2010). Efficient large-scale stereo matching. In *Asian Conference of Computer Vision*, volume 6492, pages 25–38.

Hirschmuller, H. (2008). Stereo processing by semiglobal matching and mutual information. *IEEE Trans. PAMI*, 30(2):328 –341.

Kopf, J., Lischinski, M. F. C. D., and Uyttendaele, M. (2007). Joint bilateral upsampling. *ACM Trans. on Graphics*, 26(3):96.

Lai, K., Bo, L., Ren, X., and Fox, D. (2011). A large-scale hierarchical multi-view rgb-d object dataset. In *IEEE International Conference on Robotics and Automation (ICRA)*, pages 1817–1824.

Lai, P. L., Tian, D., and Lopez, P. (2010). Depth map processing with iterative joint multilateral filtering. In *Picture Coding Symposium*, pages 9–12.

Mori, Y., Fukushima, N., Yendo, T., Fujii, T., and Tanimoto, M. (2009). View generation 3d warping using depth information for ftv. *Signal Processing: Image Communication*, 24(1–2):65–72.

Ohta, Y. and Kanade, T. (1985). Stereo by intra - and inter-scanline search using dynamic programming. *IEEE Trans. PAMI*, 7(2):139–154.

Pestschnigg, G., Szeliski, R., Agrawala, M., Cohen, M., Hoppe, H., and Toyama, K. (2004). Digital photography with flash and no-flash image pairs. *ACM Trans. on Graphics*, 23(3):664–672.

Scharstein, D. and Szeliski, R. (2002). A taxonomy and evaluation of depth two-frame stereo correspondence algorithms. *International Journal of Computer Vision*, 47(1):7–42.

Sun, J., Zheng, N. N., and Shum, H. Y. (2003). Stereo matching using belief propagation. *IEEE Trans. PAMI*, 25(7):787–800.

Tomasi, C. and Manduchi, R. (1998). Bilateral filtering for gray and color image. In *International Conference of Computer Vision*, pages 839–846.

Wildeboer, M. O., Fukushima, N., Yendo, T., Tehrani, M. P., Fujii, T., and Tanimoto, M. (2010). A semi-automatic multi-view depth estimation method. In *Proceedings of SPIE Visual Communications and Image Processing 2010*, volume 7744.

Yang, Q., Wang, L., and Ahuja, N. (2010). A constant-space belief propagation algorithm for stereo matching. In *Computer Vision and Pattern Recognition*, pages 1458–1465.

Yang, Q., Wang, L., Yang, R., Stewenius, H., and Nister, D. (2008). Stereo matching with color-weighted correlation, hierarchial belief propagation and occlusion handling. *IEEE Trans. PAMI*.

Yang, Q., Yang, R., Davis, J., and Nister, D. (2007). Spatial-depth super resolution for range images. In *Computer Vision and Pattern Recognition*, pages 1–8.

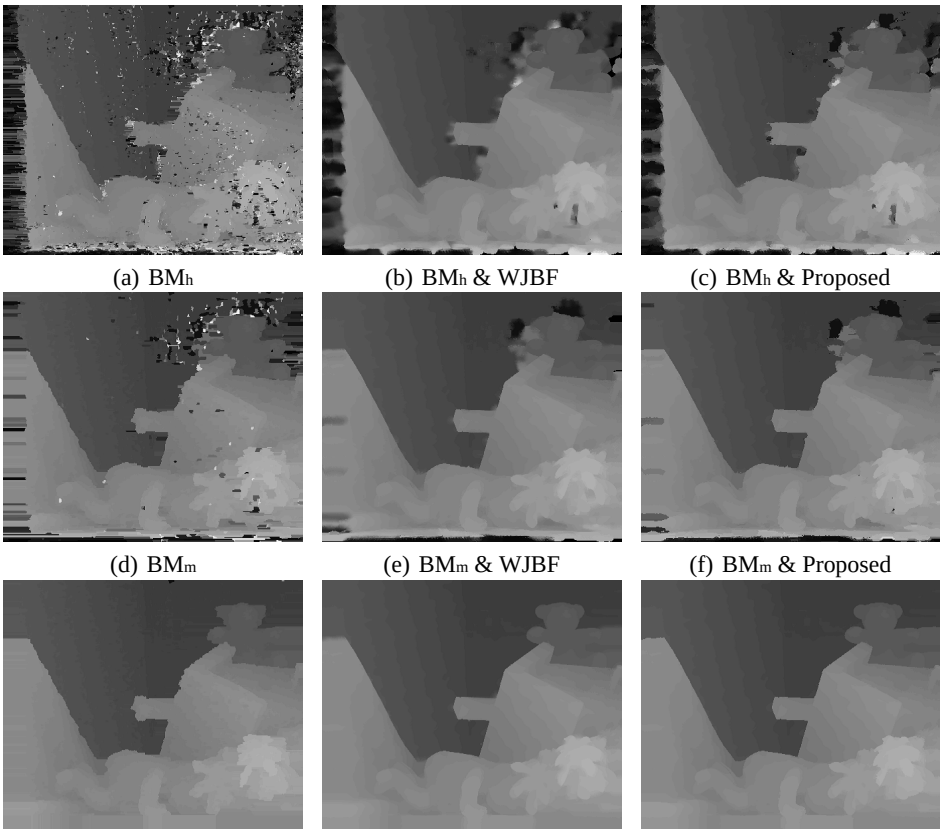

(a) BM_h (b) BM_h & WJBF (c) BM_h & Proposed

(d) BM_m (e) BM_m & WJBF (f) BM_m & Proposed

(g) BM_l (h) BM_l & WJBF (i) BM_l & Proposed

Figure 6: Results: block matching.

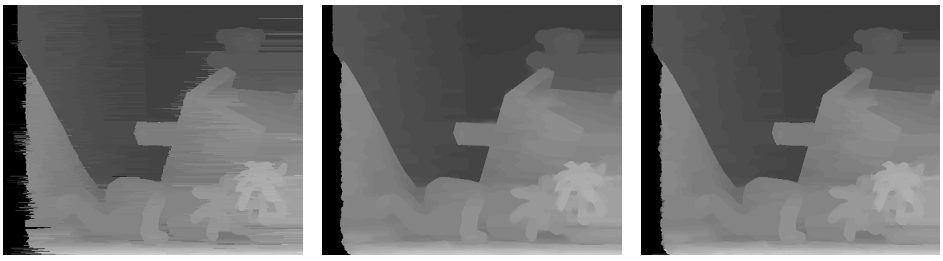

(a) DP (b) DP & WJBF (c) DP & Proposed

Figure 7: Results: dynamic programming.

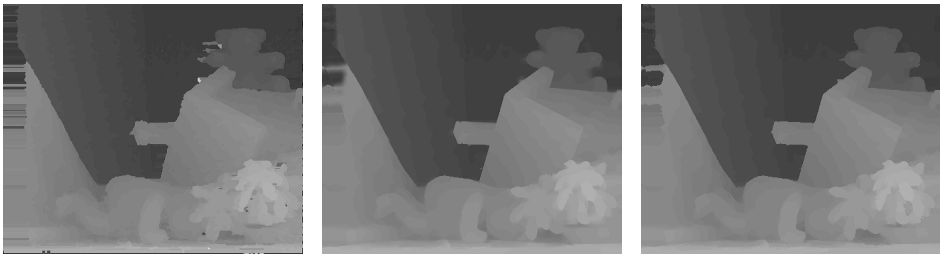

(a) SGBM (b) SGBM & WJBF (c) SGBM & Proposed

Figure 8: Results: semi-global block matching.

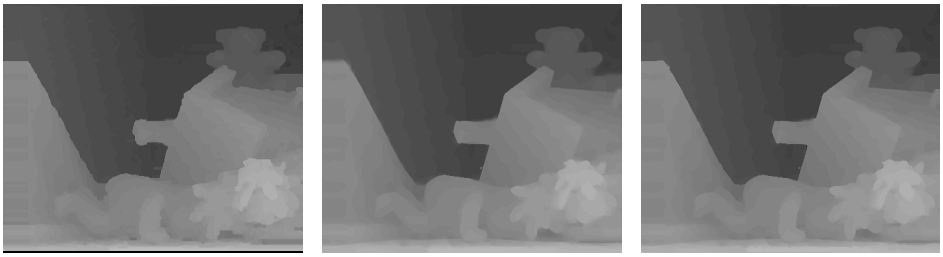

(a) ELAS (b) ELAS & WJBF (c) ELAS & Proposed

Figure 9: Results: efficient large-scale.

(a) DBP (b) DBP & WJBF (c) DBP & Proposed

Figure 10: Results: double belief propagation.

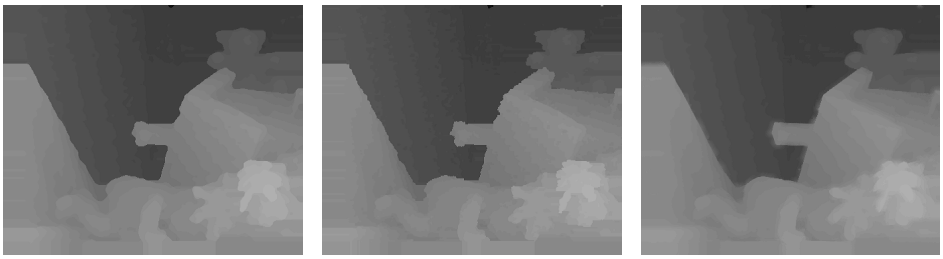

(a) MF (b) BF (c) JBF

(d) MLF (e) CSBP

Figure 11: Results: competitive refinement filters.

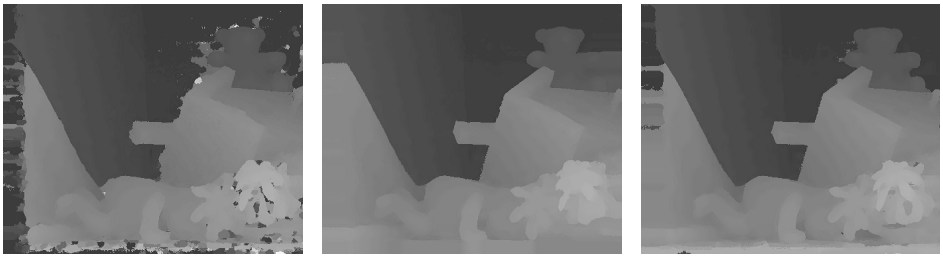

(a) BM_h & CVR (b) BM_l & CVR (c) SGBM & CVR

Figure 12: Results: cost volume refinement.